Title

A concept for mitigating head injury under translational blunt impact

Journal

International Journal of Crashworthiness, 20(5)

ISSN

1358-8265

Authors

Nazarian, O
Begley, MR
Zok, FW

Publication Date

2015-09-03

DOI

10.1080/13588265.2015.1038866

Peer reviewed

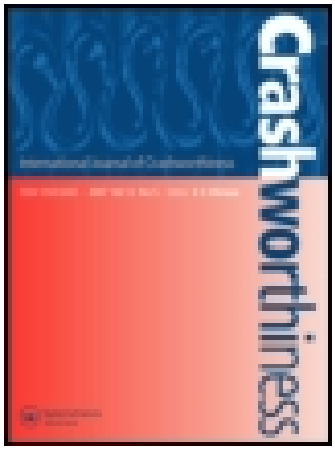

International Journal of Crashworthiness
Publication details, including instructions for authors and subscription information:
http://www.tandfonline.com/loi/tcrs20

A concept for mitigating head injury under translational blunt impact

O. Nazarian[a], M.R. Begley[a] & F.W. Zok[a]
[a] Materials Department, University of California, Santa Barbara, CA, USA
Published online: 28 May 2015.

International Journal of Crashworthiness, 2015
http://dx.doi.org/10.1080/13588265.2015.1038866

Taylor & Francis
Taylor & Francis Group

A concept for mitigating head injury under translational blunt impact

O. Nazarian *, M.R. Begley and F.W. Zok

Materials Department, University of California, Santa Barbara, CA, USA

(*Received 22 October 2014; accepted 3 April 2015*)

This study assesses a bi-layer composite concept for mitigating the severity of injury due to translational blunt impact of an unprotected head at moderately high speeds. The concept comprises crushable foam and a stiff face-sheet on the impacting face. Approximate analytical models for acceleration–time histories of prototypical impact scenarios are used to guide the design. The key design variables probed experimentally are the crushing strength of the underlying foam and the tile size. The efficacy of the composite systems and the foams alone is ascertained through a series of drop impact tests with an instrumented head-form at a representative impact velocity (6.7 m/s, 15 mph), using three commercial viscoelastic foams, with and without face-sheets. The measurements are analysed in terms of five performance metrics: the peak acceleration, the Gadd severity index (*GSI*), the head injury criterion (*HIC*), the skull fracture correlate (*SFC*) and the head impact power (*HIP*). The experiments demonstrate that, with the addition of a face-sheet, each of these metrics can be reduced substantially (by as much as a factor of two) relative to those of the foam alone. The benefits derive from spreading of contact forces over a larger area of foam by the face-sheet.

Keywords: head injury; foams; impact

1. Introduction

Head injury resulting from blunt impact of vehicle occupants in automobile collisions can be mitigated to some extent through the use of crushable foams [19,25,39]. When the design of the system is constrained by thickness (as it is in automobiles), the optimal performance is obtained when the acceleration–time history exhibits a 'top-hat' profile and nearly the full densification strain of the foam is utilised; beyond densification, the acceleration rapidly rises and leads to a significant increase in the likelihood of injury. This study examines the design and performance of layered composite systems that are potentially more effective than foams alone in mitigating head injury under severe translational (linear) impact.

Numerous metrics have been proposed to characterise severity of head impact. For purely translational impacts, the metrics are couched in terms of characteristics of acceleration–time histories experienced by the head during the impact event. Most have been derived from laboratory experiments (e.g. drop tests on cadaver heads) and from re-created real-life impact events in which the injury outcome had been well documented. Such re-creations have been performed both experimentally using instrumented test dummies [2,3,10,36,38] and by computational simulations [2–4,16,18,29,36,40]. The metrics have found utility in guiding the designs of a wide range of systems for mitigating head injury, ranging from interior cabins of transport vehicles (e.g. automobiles, airplanes and tanks) to protective head gear for motorcyclists and athletes in contact sports (e.g. football, hockey, soccer and snowboarding [12,26]), to surfaces on children's playgrounds [21,41] and for cheerleading [31]. Furthermore, they have been adopted by regulatory agencies in establishing performance standards for impact-mitigation systems.

Although metrics based on translational impacts have proven to be useful in predicting severe injury (including skull fracture and brain contusion), recent studies have highlighted the importance of angular acceleration on concussive injuries such as subdural hematomas and diffuse axonal injury [17]. Such injuries appear to arise when the strain in brain tissue exceeds a critical value [8,22,30]. Metrics based on peak angular velocity or peak angular acceleration have been proposed to characterise the severity of impacts involving rotational motion [17,32].

This study focuses on a concept for mitigating severe head injury under translational blunt impact. Recognising the limitations of the impact severity metrics, the metrics are used in a largely comparative manner, with the goal of ranking the protection capabilities of various candidate systems. Additionally, to minimise bias, five different metrics are used for making these rankings. However, for the specific tests reported here, the metrics are found to be highly correlated with one another; within the resolution

*Corresponding author. Email: oshin@engineering.ucsb.edu

of the measurements, they follow monotonic (nearly proportional) trends. In light of this result, one such criterion – the head injury criterion (*HIC*) – is employed in conjunction with analyses of acceleration–time histories of prototypical translational impact events, to glean insights into the design of such systems. Although approximate, the analyses prove to yield designs that are indeed superior in terms of all five performance metrics. They also yield insights into the mechanics governing the efficacy of protection.

Numerous studies performed over the past half-century have revealed strong correlations between measures of impact severity based on linear acceleration–time histories and the degree of head and/or brain injury. The measures originated through impact studies on skulls of human cadavers and live animals [13]. The early data were used to construct the so-called Wayne State Tolerance Curve: the locus of average acceleration and impact duration below which skull fracture would not occur. A stronger correlation of these and other test results was obtained using measures of impact severity based on weighted averages of acceleration–time profiles. The first of these was the Gadd severity index (*GSI*) [11], defined by

$$\mathrm{GSI} = \int_0^{t_*} [a(t)]^{5/2} dt, \tag{1}$$

where a is deceleration in units of g (the acceleration due to gravity), t is time and t_* is the impact duration.

Yet, a stronger correlation was obtained using the *HIC*, defined by [6,11,13,14,34]

$$\mathrm{HIC} = \max_{t_1,t_2} \left\{ \left[\frac{\int_{t_1}^{t_2} a(t)dt}{t_2 - t_1} \right]^{5/2} (t_2 - t_1) \right\}, \tag{2}$$

where t_2 and t_1 are the two times that maximise the quantity in $\{...\}$, subject to the constraint that the two times do not differ from one another by more than a prescribed amount, t_c (typically, 15 ms) (Figure 1). The *HIC* is essentially a product of a power-weighted time-averaged acceleration and the corresponding time duration. Because of the weightings, the *HIC* is more sensitive to acceleration than time duration. The time restriction reflects the fact that low acceleration levels over extended periods of time pose low risk of injury. The *HIC* remains the most popular of the available metrics. It is used by the automotive, aviation and sports industries [5,9,12,20,26,28,31] as well as the governing regulatory agencies, *e.g.* US National Highway Traffic Safety Administration [33], US Insurance Institute for Highway Safety [15] and US Federal Aviation Administration [7]. It was subsequently proposed for use in predicting brain injury (without skull fracture) during head contact in professional football, with moderate success [24].

More recently, two other metrics have been proposed. The first is the skull fracture correlate (*SFC*) [35]. It is defined as the average acceleration over the *HIC* time interval (from t_1 to t_2), expressed formally as

$$\mathrm{SFC} = \frac{\int_{t_1}^{t_2} a(t)dt}{t_2 - t_1}. \tag{3}$$

The *SFC* was initially proposed to rationalise the results of a series of drop tests of instrumented post-mortem human heads over a velocity range of 2–10 m/s at targets of varying hardness [35]. X-ray radiographs and computed tomography images taken after tests at progressively increasing drop speeds were used to identify the onset of skull fracture. Additionally, finite element simulations of the impacts yielded maximum principal strains in the skull that correlated closely with the *SFC*. The latter results were used to argue for the biofidelity of the *SFC*.

The other is the head impact power (*HIP*). For a normal impact without angular momentum, it is defined by

$$\mathrm{HIP} = \max \left\{ m\, a(t) \int_{t_s}^{t} a(\bar{t}) d\bar{t} \right\}, \tag{4}$$

where t_s is the starting time of the impact and m is the mass of the head. The quantity within $\{\ldots\}$ is evaluated for all times $t > t_s$; the maximum value of this function defines the *HIP*. For non-normal impacts (with, generally, three linear acceleration components) and when angular momentum is finite (again, generally, with three components), corresponding terms for each component can be added linearly to the one on the right-hand side of Equation (4). The *HIP* has been found to be useful in correlating the incidence of mild traumatic brain injury in professional football players following head impact [27] as well as accidents involving motorcyclists and pedestrians [23].

In the experimental portion of this study, each of the four preceding metrics is computed for each impact event and is used in assessing impact severity. For completion, the maximum linear acceleration, $a_{\max}$, is also recorded.

An analytical model for assessing the efficacy of crushable foams in mitigating the HIC for representative impact scenarios has been presented elsewhere [1]. The model is based on an analysis of impact of a spherical mass onto a target of flat crushable foam. The form of the resulting acceleration–time history is shown schematically in Figure 1(a). (Pertinent details are presented in the following section.) Here, the contact area between the spherical mass and the foam target increases progressively

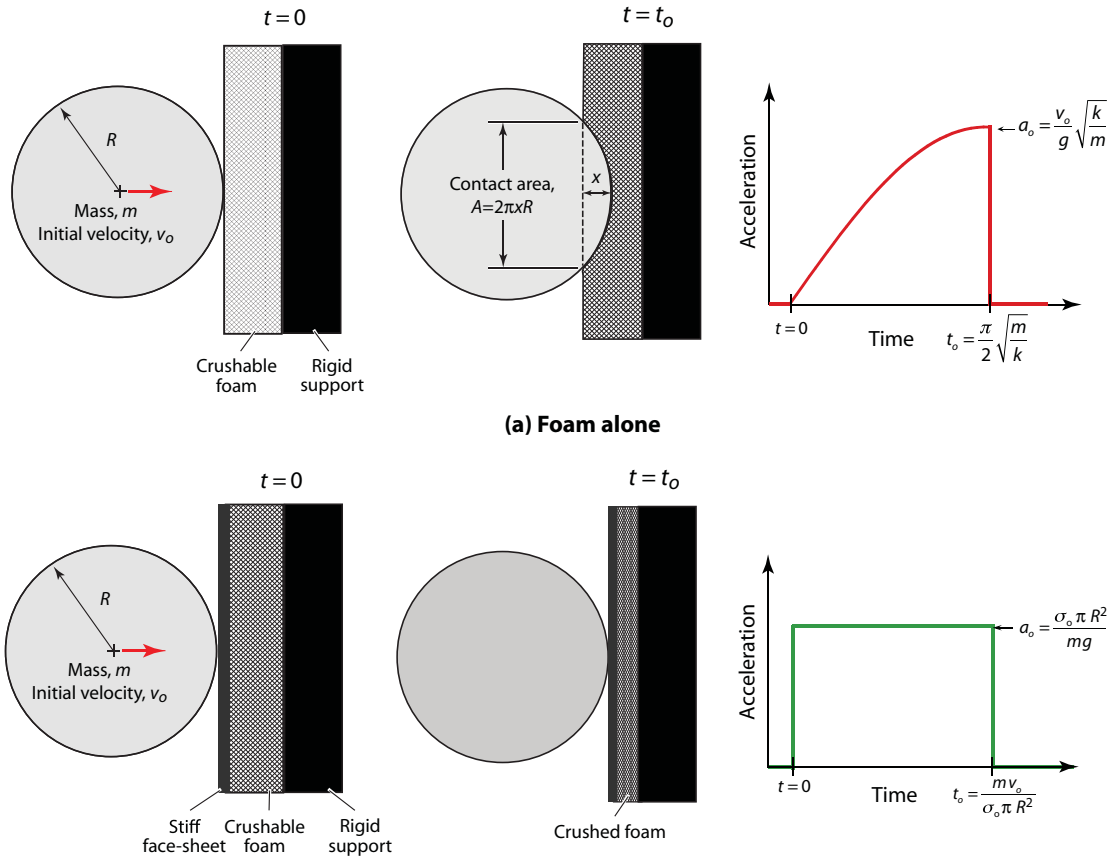

Figure 1. Two impact scenarios, based on (a) a crushable foam tile mounted on a rigid support and (b) a face-sheet/foam composite, also mounted on a rigid support.

with increasing penetration depth; the acceleration varies with depth accordingly. The model is used here to identify the optimal foam strength that minimises the severity of impact (as characterised, for example, by the HIC) for prescribed head mass and impact velocity, subject to constraints on foam thickness.

The concept under consideration in this study is illustrated in Figure 1(b). It comprises a foam tile and a thin stiff face-sheet on the impacting surface. It is predicated on the notion that, provided plate bending is small, the impact load should be spread uniformly throughout the foam over the area defined by the plate dimensions. The expectation then is that the force resisting impact and the acceleration of the impacting head would be essentially constant over the duration of the event (shown on the right-hand side of Figure 1(b)). For prescribed values of mass and impact velocity (and hence prescribed incident momentum), a uniform acceleration is expected to yield lower values of the various impact severity metrics than those obtained for a progressively rising acceleration. This occurs because the metrics exhibit a stronger sensitivity to acceleration than to the impact duration.

The principal objective of this study is to assess the benefits of face-sheets on foams in reducing the severity of head impact during a translational impact. Approximate analytical models are developed for the linear acceleration–time histories of an impacting head-form onto foam targets both with and without face-sheets. In turn, the analytical results are used to guide the design of a series of idealised targets for the experimental study. The efficacy of the proposed concept is assessed through drop tests of an instrumented head-form at a representative impact speed, notably 6.7 m/s. (This speed is used by the US Department of Transportation in the Federal Motor Vehicle Safety Standards [31]). The test results show that the benefits of the face-sheet can indeed be significant, with the impact severity metrics being reduced by as much as a factor of two.

2. Analytical models of impact

2.1. *Foam targets*

Approximate analytical solutions are presented for the acceleration–time histories for the two impact scenarios

shown in Figure 1. Here, the head is treated as a rigid spherical body of radius R and mass m. In the first scenario, the spherical body makes impacts a foam tile of thickness H_o at a velocity v_o. The foam is presumed to be rigid/perfectly plastic with a rate-independent crushing stress σ_o up to the densification strain ε_D . The foam tile is further taken to be sufficiently thick so that full densification does not occur before the mass arrests.

Provided the displacement $x \ll R$, the contact area A_c is given approximately by $A_C \approx 2\pi Rx$ and thus the contact force is $F = 2\pi Rx\sigma_o$. Solving the equation of motion of the spherical mass yields the variations in position *x(t)*, velocity *v(t)* and acceleration *a(t)* with time *t*. These are given by

$$x(t) = v_o\sqrt{\frac{m}{2\pi R\sigma_o}}\sin\sqrt{\frac{2\pi R\sigma_o}{m}}t, \tag{5}$$

$$v(t) = v_o\cos\sqrt{\frac{2\pi R\sigma_o}{m}}t, \tag{6}$$

$$a(t) = \frac{-\ddot{x}}{g} = \frac{v_o}{g}\sqrt{\frac{2\pi R\sigma_o}{m}}\sin\sqrt{\frac{2\pi R\sigma_o}{m}}t, \tag{7}$$

over the time domain

$$0 \le t \le t_o = \frac{1}{2}\sqrt{\frac{\pi m}{2R\sigma_o}}. \tag{8}$$

For $t \ge t_o$, $x(t) = v_o\sqrt{m/2\pi R\sigma_o}$, $v(t) = 0$ and $a(t) = 0$ (Figure 1(a)). Thus, the peak acceleration and peak displacement, obtained at $t = t_o$, are

$$a_{\max} = \frac{v_o}{g}\sqrt{\frac{2\pi R\sigma_o}{m}} \tag{9}$$

and

$$x_{\max} = v_o\sqrt{m/2\pi R\sigma_o}. \tag{10}$$

In order for arrest to precede densification, the foam thickness must exceed a critical value, given by

$$H_o = \frac{x_{\max}}{\varepsilon_D} = \frac{v_o}{\varepsilon_D}\sqrt{\frac{m}{2\pi R\sigma_o}}. \tag{11}$$

As intimated earlier and demonstrated by subsequent test results, the five metrics – *GSI*, *HIC*, *HIP*, *SFC* and $a_{\max}$ – are highly correlated with one another for the impact events of present interest. As a result, comparative rankings of the various test systems from each of the metrics are essentially the same. In light of this, the subsequent analysis focuses on only one of these metrics: notably, the *HIC*.

The *HIC* is evaluated using Equation (2). Here, $t_2 = t_o$ and t_1 is obtained by maximising the quantity within $\{...\}$ in Equation (2). It has the solution

$$t_1 = 0.518\sqrt{\frac{m}{2\pi R\sigma_o}} = 0.33t_o. \tag{12}$$

Combining Equations (2), (7), (8) and (12) yields

$$\mathrm{HIC} = 0.651\left(\frac{2\pi R\sigma_o}{m}\right)^{3/4}\left(\frac{v_o}{g}\right)^{5/2}. \tag{13}$$

The minimum *HIC* value and the corresponding optimal foam strength are obtained when the foam thickness is equal to its minimum critical value. From Equations (11) and (13), they are

$$\mathrm{HIC}_{\min} = \frac{1.84\,v_o^4}{(2H_o\varepsilon_D)^{3/2}g^{5/2}}, \tag{14}$$

$$\sigma_o^{\mathrm{opt}} = \frac{mv_o^2}{2\pi R(H_o\varepsilon_D)^2}. \tag{15}$$

2.2. *Bi-layer targets of face-sheet and foam*

The potential benefit of a stiff face-sheet on the contacting surface of a foam target is estimated through an analogous analysis. Provided the face-sheet experiences minimal bending during the impact, the load is distributed *uniformly* over the entire area A_t of the tile. Furthermore, provided the arrest precedes foam densification, the solution to the equation of motion is simply:

$$a = a_o = \frac{\sigma_o A_t}{mg}, \tag{16}$$

over the time interval

$$0 \le t \le t_o = \frac{mv_o}{\sigma_o A_t}. \tag{17}$$

The two times that maximise HIC are $t_1 = 0$ and $t_2 = t_o$. Integrating Equation (2) yields:

$$\mathrm{HIC} = \left(\frac{\sigma_o A_t}{mg}\right)^{3/2}\left(\frac{v_o}{g}\right). \tag{18}$$

Following optimisation, the minimum HIC and the optimal foam strength become:

$$\mathrm{HIC}_{\min} = \frac{v_o^4}{(2H_o\varepsilon_D)^{3/2}g^{5/2}} \tag{19}$$

and

$$\sigma_o^{\text{opt}} = \frac{mv_o^2}{A_t H_o \varepsilon_D}. \tag{20}$$

Equation (20) can be interpreted equivalently as the optimal tile area A_t^{opt} for a prescribed foam strength σ_o.

Comparison of Equations (14) and (19) shows that, in theory, the HIC can be reduced by a factor of $1/1.84 \approx 0.54$ through the addition of a stiff load-spreading face-sheet. This prediction motivates the following experimental programme.

3. Materials and test procedures

Tests were conducted on three viscoelastic polyurethane foams (SunMate®, Dynamic Systems Inc., Leicester, NC). The manufacturer's designations for these foams are Firm, X-Firm and XX-Firm. (These foams are typically used for wheelchair seat cushions, aircraft ejection seats and race-car impact padding [25].) The quasi-static compressive stress–strain response of the foams is shown in Figure 2. The materials were procured as plates with a thickness of 38.1 mm and a density of approximately 88 kg/m^3. Square specimens of varying sizes (75–150 mm) were cut from the plates using a precision table saw. Square specimens of equal size were cut from 3.3 mm thick sheets of a [0°/90°] carbon fiber-reinforced plastic (CFRP). For tests conducted on foam/CFRP composites, the sheets had been adhered to the foam using an epoxy resin (Devcon®, Danvers, MA).

Free-fall impact tests were performed using an Al-alloy 'missile' as a surrogate head-form, in accordance with American Society for Testing and Materials (ASTM) Standard F1292 [41]. This head-form has a mass of 4.6 kg and a spherical nose with a radius of 80 mm (Figure 3). The head-form is instrumented with a triaxial accelerometer. It was mounted in a tripod drop system (Triax 2010, Alpha Automation Inc, Ewing Township, NJ) and dropped from a height of 2.3 m, yielding an impact velocity of 6.7 m/s (15 mph). An electro-magnetic release mechanism was employed to allow smooth (rotation-free) release from the tripod. The test specimens were affixed to the ground around their periphery using duct tape. Side-view images were recorded with a high-speed video camera (Phantom v7, Vision Research®, Wayne, NJ) placed at a height level with the top of the foam. The videos were used to corroborate both the predicted impact velocities (based on drop height) and the displacements computed by integration of the accelerometer data. Either two or three tests were performed on each foam and foam/CFRP composite. The results were found to be very reproducible, yielding HIC values within about 5% of one another. (Parenthetically, HIC values obtained using a rigid Al alloy head-form are reportedly slightly higher than those obtained using head-forms with life-like properties [41]. In this respect, the present tests should yield conservative results.)

A series of preliminary tests was performed to identify the appropriate sizes of the composite specimens. From Equation (20), the optimal tile area is expected to scale inversely with foam strength. This led to the selection of smaller tiles for the stronger foams and vice versa. Specifically, tile dimensions of 150 mm × 150 mm were used with both the Firm and the X-Firm foams, 100 mm × 100 mm for both the X-Firm and XX-Firm foams, and 75 mm × 75 mm and 89 mm × 89 mm for the XX-Firm foam. It should be noted that because the models presented here are rudimentary and approximate – neglecting effects of face-sheet bending, elastic recovery and strain rate sensitivity – they are used only to *guide* the

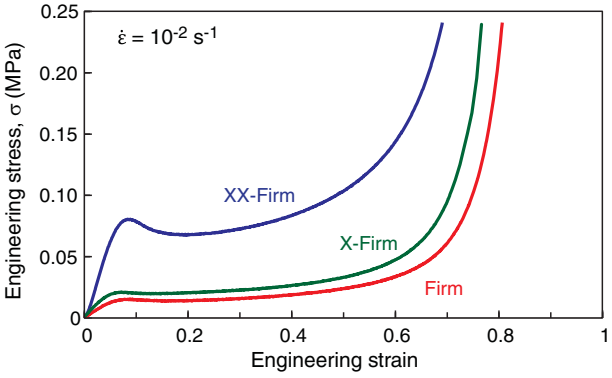

Figure 2. Representative compressive stress–strain curves for SunMate® foams under quasi-static loading.

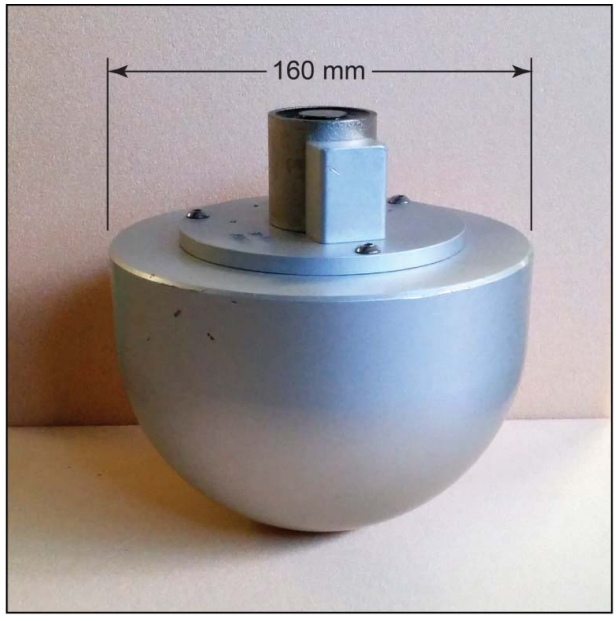

Figure 3. Al alloy 'missile' used as surrogate head-form with the Triax 2010 drop test system.

design. Optimisation would require more rigorous computational simulations of such impacts.

4. Impact results: experimental measurements and model predictions

Representative acceleration–time and displacement–time histories measured on the foams and the foam/CFRP composite tiles are shown in Figure 4. The displacements (measured relative to the point of initial contact) are normalised by the thickness of the foam tile and thus represent the maximum nominal strain beneath the contact site.

The results for the foams alone (Figures 4(a) and 4(b)) exhibit the following characteristics. (1) The initial rise of the acceleration–time curve scales roughly linearly with the quasi-static foam strength, in accordance with Equation (7). (2) For the two softer foams, the initial nearly linear rise is followed by a rapid upturn in acceleration, to a peak value of 250–290 g. The upturn is attributable to full densification of the foam and 'bottoming out' of the head-form, as evidenced by a peak displacement $x_{max}/H_o \geq 0.9$ (Figure 4(b)). (3) The strongest foam does not exhibit an upturn in acceleration rate, consistent with the peak displacement being less (albeit only slightly) than that needed for significant densification. Consequently, the peak acceleration is reduced to about 160 g and the *HIC* is reduced from 1500 (for the softest foam) to 900 s. Furthermore, the curve shape (up to the peak) is broadly consistent with that predicted by Equation (7) and plotted in Figure 1(a).

For the foam/CFRP composite tiles, the acceleration rises sharply to a plateau and then gradually increases to the peak (Figure 4(c)). The peak accelerations and *HIC* values are lower than those of the foam alone. The effects are most pronounced for the softest foam: the peak acceleration dropping from 290 to 120 g and the *HIC* dropping from 1500 to 750 s. Here, again the peak displacements are maintained below the levels needed for significant densification (Figure 4(d)).

Correlations between the five metrics for impact severity are shown in Figure 5. Here, the results are plotted as *GSI, SFC, HIP* and a_{max} vs. *HIC*. The metrics not only appear to vary monotonically but are also close to being proportional to one another. Thus, for the present test results, halving of the peak acceleration is accompanied by halving of the *HIC*, the *SFC*, the *HIP* and the *GSI*. An important implication is that comparative rankings of the various test systems can be achieved with any one of the five metrics.

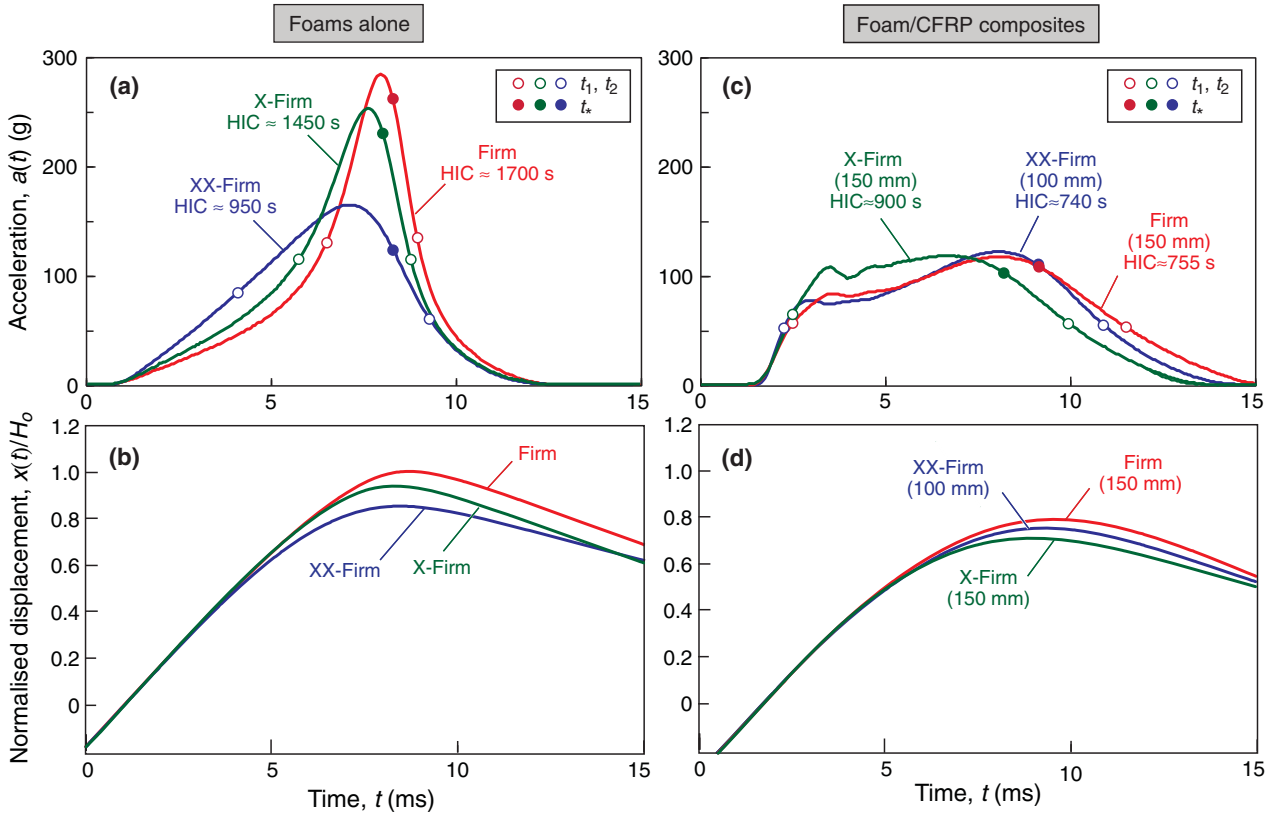

Figure 4. Experimental impact test results for (a) and (b) foams alone (150 mm × 150 mm tiles) and (c) and (d) foam CFRP composites (tile sizes indicated). Also shown in (a) and (b) are the two times t_1 and t_2 bounding the *HIC* calculation (indicated by open symbols) and the time t_* at which rebound commences (solid symbols).

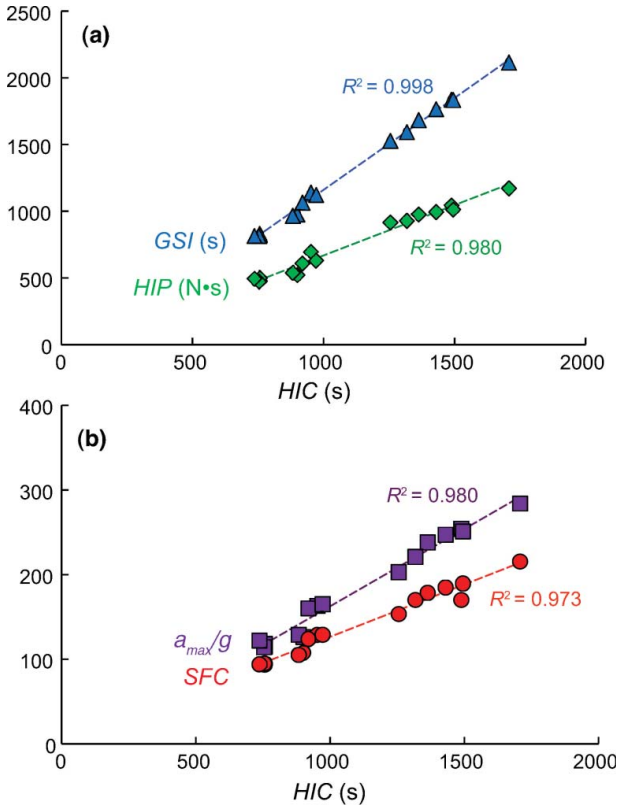

Figure 5. Correlation between the five metrics used to assess severity of impact. (R is the correlation coefficient for a linear fit of the data.)

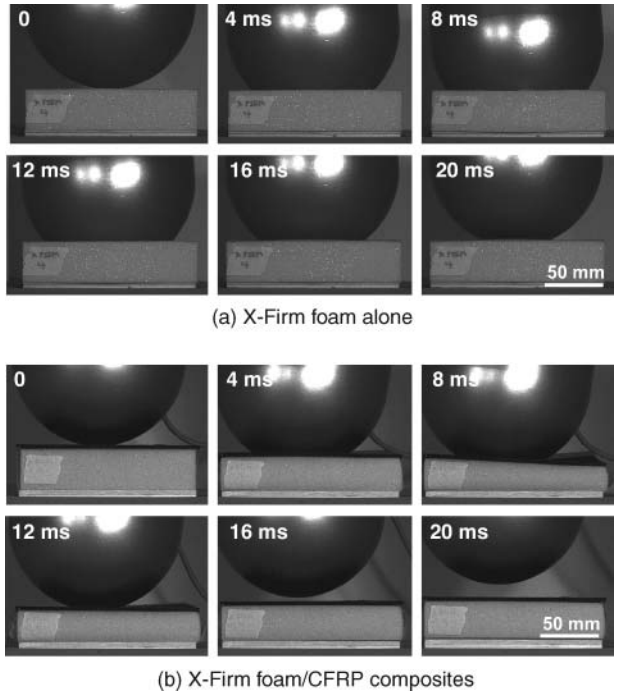

Figure 6. Image sequences showing representative impacts of head-form onto (a) the X-Firm foam alone and (b) the X-Firm foam with the added face-sheet. Both tiles are 150 mm × 150 mm. Slight but detectable bending and twisting of the CFRP plates are evident in (b) the effects are elastic and hence recoverable.

Representative side-view images taken via high-speed video for a test on the foam alone and a foam/CFRP composite are shown in Figure 6. Deformation of the foam alone is localised to the impact area; that is, the distal regions (say, 50 mm away from the impact centre) do not undergo any apparent deformation. One implication is that the test results should be representative of the performance of larger foam tiles. The deformation of the foam/CFRP composite tiles differs dramatically. Here, the foams are essentially uniformly crushed during the impact. Some plate bending and twisting are evident (the latter due to the anisotropy of the in-plane elastic properties of the CFRP), though their magnitudes are small relative to the average (total) displacement of the face-sheets and the underlying foams. These observations, combined with the nearly constant crushing stress of the foams, indicate that an approximately constant acceleration should be obtained over most of the impact duration, consistent with the test results in Figure 4(c).

Some insights into the effects of rebound of the head-form are gleaned from two additional test parameters. The first is the ratio of the rebound velocity v_r to the initial (impact) velocity v_o. The results are plotted in Figure 7(a). The quantity v_r/v_o represents the fractional increase in the imparted momentum relative to the incident value. For both the foams alone and the foam/CFRP composite tiles, v_r/v_o is about 0.3 and exhibits only a weak sensitivity to the foam strength or the presence/absence of the CFRP sheet. The second parameter considers the times (t_1 and t_2) bounding the *HIC* calculation and the time t_* at which the head-form velocity reaches zero and the head-form begins its rebound. The expectation is that, if the latter event occurs outside the pertinent interval (i.e. $t_* > t_2$), the rebound phase should have minimal effect on the *HIC*. Otherwise, if $t_1 < t_* < t_2$, the relative time duration within the *HIC* interval occupied by the rebound phase can be characterised by a non-dimensional parameter, τ_E, defined by

$$\tau_E = \frac{t_2 - t_*}{t_2 - t_1} \tag{21}$$

Figure 7(b) shows the variation of τ_E with foam strength. For both the foams alone and the foam/CFRP composites, $\tau_E \approx 0.2$, decreasing only slightly with increasing foam strength. The low values of τ_E coupled with the small fractional increase in momentum due to rebound (0.3) indicate that the rebound plays only a small (though perhaps not insubstantial) role in the *HIC* value. They are further consistent with the *asymmetry* of the acceleration−time histories (Figure 4); if foam elasticity

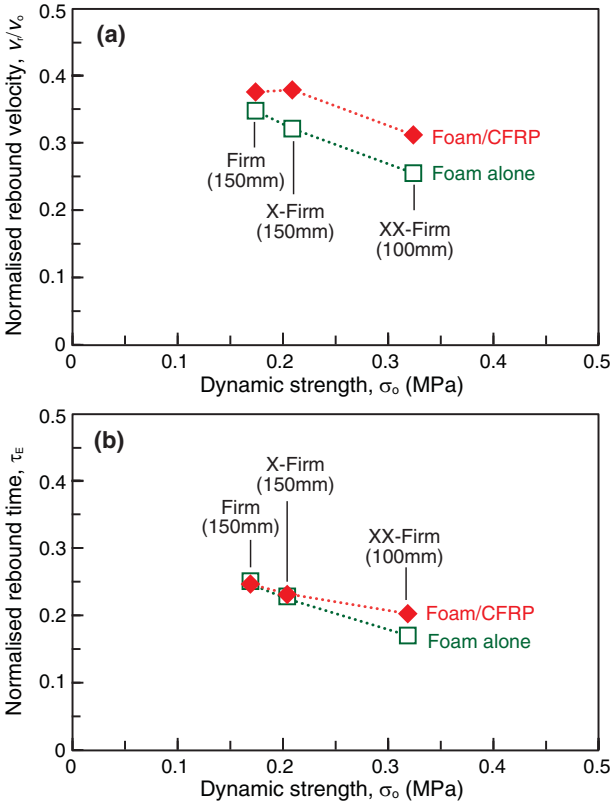

Figure 7. Effects of rebound: (a) normalised rebound velocity and (b) fractional time within the *HIC* interval spent in the rebound phase. The dynamic foam strengths were obtained from the results in Figure 8, at a compressive strain of 0.3.

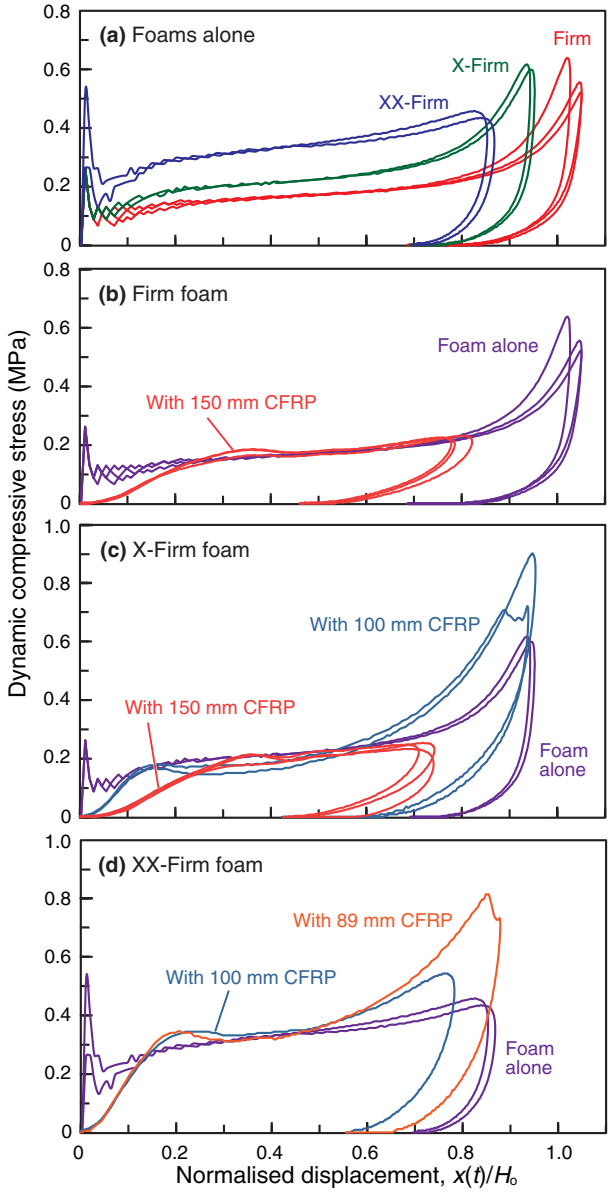

Figure 8. Dynamic compressive response of foams, inferred from impacts on both the foams alone and the foam/CFRP composites. The apparent oscillations in the stress–strain curves for the foams alone at small strains and the apparent peak in the very early stages are manifestations of errors in the calculated stresses, resulting from the infinitesimal contact areas in these early stages.

dominated the impact response, the acceleration–time histories would be perfectly symmetric about the peak.

A further assessment of the acceleration–time histories is made on the basis of the stresses experienced by the foams. For instance, since the predicted force acting on the foam (without a face-sheet) is $F = A_c\sigma_d = 2\pi Rx(t)\sigma_d = mga(t)$, the average dynamic contact stress σ_d acting on the foam is expected to be

$$\sigma_d = \frac{mga(t)}{2\pi Rx(t)}. \tag{22}$$

The dynamic contact stresses computed this way are plotted against the nominal strain $x(t)/H_o$ in Figure 8(a). The curves exhibit features similar to those of the quasi-static stress-strain curves (Figure 2), including a nearly constant crushing stress over much of the straining history and a rapid rise as densification proceeds. The stress levels, however, are higher than those associated with the quasi-static tests, by factors of about 4–10: a consequence of the intrinsic strain rate sensitivity of the foam material coupled with the inertial stabilisation against buckling of the constituent struts. Comparable (sevenfold) elevations in crushing stress have been reported recently for lattices deformed over a similar range of strain rates [37].

An analogous procedure is employed to infer the dynamic crushing stresses in the foam tiles beneath the CFRP sheets. In this case, the stress is presumed to be distributed uniformly over the tile area so that the dynamic

stress is given by

$$\sigma_d = \frac{mga(t)}{A}. \tag{23}$$

The resulting dynamic stress–strain curves inferred from the impact tests on the composite tiles are plotted in Figures 8(b)–8(d) for each of the three foams. Also reproduced on these figures are the corresponding results from the impact tests on the foams alone (from Figure 8(a)). The two sets of curves show similar features (qualitative and quantitative) with one notable exception: the initial rise in the stress–strain curves in the composite tiles is shallower than that on the foams alone and thus the attainment of the crushing plateau is obtained at seemingly high strains (of the order of 0.2). This anomalous feature is attributed to the non-uniformity in the stresses within the foams in the early stages of loading during which the plates undergo some bending and twisting (as evidenced by the images in Figure 6). The similarities in the inferred crushing stresses from the two test types support the assumptions underlying the models used to derive Equations (19) and (20). Additionally, the large hysteresis in the stress–strain curves is consistent with the earlier conclusion about the small role of elastic rebound on the severity of the impact.

The *HIC* values for the foams alone and the foam/face-sheet composites are plotted against the dynamic foam crushing stress (taken from Figure 8 at a strain of 0.3) in Figures 9(a) and 9(b), respectively. Also shown are the predictions of the analytical models: Equation (13) for the foams alone and Equation (18) for the foam/CFRP composites. The model predictions are shown only in the domain in which full densification (taken as the point at which the strain reaches 0.8) does not occur. This domain is characterised by a rising *HIC* with increasing foam strength. Full densification and head-form 'bottoming out' at low foam strengths lead to an increase in *HIC*: a feature not captured by the present models. Nevertheless, the curves in this domain would be expected to exhibit negative slope (decreasing *HIC* with increasing foam strength).

The measured *HIC* values for the foams decrease with increasing foam strength. Upon extrapolating the data to slightly higher crushing stresses, the expected *HIC* appears to correspond closely with the minimum predicted value (shown by the open circle). The implications are twofold. First, the *HIC* could be reduced slightly (relative to the strongest foam) by increasing the crushing stress by about 30% (from 0.3 to 0.4 MPa). Second, upon increasing the foam strength further (beyond 0.4 MPa), the *HIC* is expected to begin to rise. Thus, it appears that the XX-Firm foam is not too far off of optimal for the present loadings (i.e. mass, radius and velocity of head-form) and the selected foam thickness (38 mm).

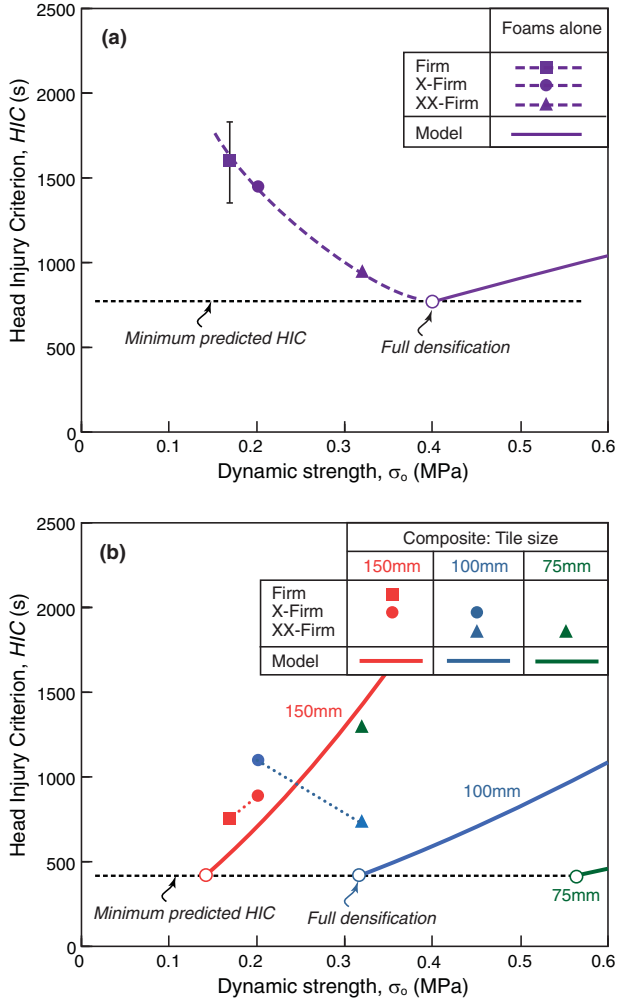

Figure 9. Variation in *HIC* with dynamic foam strength for (a) foams alone and (b) foam/CFRP composites, from experimental measurements (filled symbols) and model predictions (solid lines). Open symbols are predicted *HIC* values upon densification of the foam (at a strain of 0.8).

The trends for the foam/CFRP composites appear to be more nuanced. For the largest tiles (150 mm × 150 mm), the measurements appear to lie in the domain in which the *HIC* is rising with increasing foam strength. In this case, some reduction in *HIC* might be achieved with the use of slightly softer foam. In contrast, for the intermediate-sized and smallest tiles [100 mm × 100 mm and 75 mm × 75 mm)], the measurements appear to lie in the domain of decreasing *HIC*. A more quantitative assessment of the measurements awaits more rigorous analysis of these types of impacts.

5. Discussion and conclusions

A new concept that has the potential for mitigating head injury under translational blunt impact has been presented. It is motivated by the differences in the predicted

acceleration−time histories obtained in two idealised loading scenarios: one involving impact of a rigid spherical body onto a rigid perfectly plastic crushable foam (wherein the contact area increases progressively with penetration depth) and a second in which the impact load is spread uniformly over a prescribed area by a thin stiff face-sheet. The minimum *HIC* values for systems optimised for these two idealised scenarios differ by almost a factor of two. The efficacy of the concept has been assessed by comparing computed values of *HIC*, *SFC*, *HIP*, *GSI* and a_{max} for several commercial foams and several foam/CFRP composites, at an impact velocity relevant to vehicle occupants in automobile collisions. The key conclusions follow.

(1) The performance metrics are highly correlated and nearly proportional to one another in the present tests. Thus, comparative rankings (qualitative and quantitative) of the various test systems can be made on the basis of any one of these metrics.
(2) Among the foams tested, the XX-Firm performs best, with a *HIC* of 950 s. By comparison, the predicted minimum is about 700 s for the prescribed foam thickness (38 mm) and impact velocity (6.7 m/s).
(3) The models indicate that, with the addition of a stiff face-sheet on the impacting face of a foam tile, the predicted minimum in *HIC* is about half that of an optimal foam tile alone. Reductions in *HIC* of roughly this magnitude have indeed been obtained in some of the systems examined here. Additional work is needed to address the performance of composite tiles for impacts that occur away from the tile centreline.
(4) The effects of elastic rebound on the *HIC* measurements appear to be small. The rebound phase comprises only a small part of the pertinent duration of the impact event (over which the *HIC* is computed) and the rebound velocity is a moderate fraction of the incident velocity.

In closing, we make three qualifications regarding this study. First, the impact locations in the tests were selected to coincide with the tile centres. For the foams alone, the test results are expected to be representative of semi-infinite tiles; this expectation is based on the observation that negligible deformation was obtained in regions remote from the impact site, even for the rather modest tile sizes employed. For the foam/CFRP targets, the impact behaviour is expected to vary somewhat with the location of the impact relative to the tile centre or tile edges, because of the asymmetry of loading. Consequently, a periodic array of abutting composite tiles – a potential solution for large-acreage impact-mitigation systems – might give rise to spatial variations in impact severity. One possible solution to this problem would entail use of overlapping face-sheets. This concept has yet to be assessed.

Second, in making comparisons between the two target types (with and without face-sheets), the effect of the face-sheet thickness on the total target thickness had been neglected. That is, if the total thickness had been restricted to, say, 38 mm, then the underlying foam bases for the composite tiles would need to be reduced from their initial thickness by an amount equal to the face-sheet thickness. In the present experiments, the face-sheet represents about 9% of the total. Such effects are likely to be small but finite when making more rigorous comparative assessments.

Third, although the correspondence between the experimental measurements and the theoretical predictions appears reasonable, there remains a need to perform more rigorous analyses that account for the effects of the strain rate sensitivity of the foam strength, the finite strain hardening of the foams at strains approaching densification and the effects of elastic bending and rebound of the face-sheets.

Acknowledgements

This work was supported by the Institute for Collaborative Biotechnologies through grant W911NF-09-0001 from the US Army Research Office. The content of the information does not necessarily reflect the position or the policy of the Government and no official endorsement should be inferred.

Disclosure statement

No potential conflict of interest was reported by the authors.

Funding

This work was supported by the Institute for Collaborative Biotechnologies [grant W911NF-09-0001] from the US Army Research Office.

Note

1. Although this study was not designed to address specific applications, the foam thickness (38 mm) selected for the experimental portion is broadly consistent with the expected allowable thickness of impact protection systems for cabin interiors of automobiles (∼25−50 mm). Similarly, the impact velocity was selected to be consistent with the test standards employed by the National Highway Traffic Safety Administration.

ORCID

O. Nazarian http://orcid.org/0000-0002-5003-3164

References

[1] M.R. Begley and F.W. Zok, *Optimal material properties for mitigating brain injury during head impact*, J. Appl. Mech. 81 (2013), pp. 031014-031014-5.

[2] A. Cazon and A. Suescun, *Head injuries due to unrestrained objects during frontal collisions*, Int. J. Crashworthiness 15 (2010), pp. 39–48.

[3] C.Z. Cory and M.D. Jones, *Development of a simulation system for performing in situ surface tests to assess the potential severity of head impacts from alleged childhood short falls*, Forensic Sci. Int. 163 (2006), pp. 102–114.

[4] C. Deck and R. Willinger, *Improved head injury criteria based on head FE model*, Int. J. Crashworthiness 13 (2008), pp. 667–678.

[5] R.L. Deweese and D.M. Moorcroft, *Evaluation of a Head Injury Criteria Component Test Device*, Report No. DOT/FAA/AM-18, Department of Transportation,Washington, DC, 2004.

[6] A.M. Eiband, *Human tolerance to rapidly applied accelerations: A summary of the literature*, NASA Memo. 5-19-59E (1959).

[7] Federal Aviation Administration, *Federal Aviation Regulations, Part 25 – Airworthiness Standards: Transport Category Airplanes, SFAR No. 109*, US Government Printing Office, Washington, DC, 2014.

[8] Y. Feng, R.J. Okamoto, R. Namani, G.M. Genin, and P.V. Bayly, *Measurements of mechanical anisotropy in brain tissue and implications for transversely isotropic material models of white matter*, J. Mech. Behav. Biomed. Mater. 23 (2013), pp. 117–132.

[9] C. Fremgen, L. Mkrtchyan, U. Huber, and M. Maier, *Modeling and testing of energy absorbing lightweight materials and structures for automotive applications*, Sci. Technol. Adv. Mater. 6 (2005), pp. 883–888.

[10] S.I. Fuhrman, P.E. Karg, and G.E. Bertocci, *Effect of wheelchair headrest use on pediatric head and neck injury risk outcomes during rear impact*, Accident Anal. Prevention 40 (2008), pp. 1595–603.

[11] C.W. Gadd, *Use of a weighted-impulse criterion for estimating injury hazard*, Proceedings of the 10th Stapp Car Crash Conference, Society of Automotive Engineers, New York, NY, 1966, pp. 164–174.

[12] R.M. Greenwald, J.T. Gwin, J.J. Chu, and J.J. Crisco, *Head impact severity measures for evaluating mild traumatic brain injury risk exposure*, Neurosurgery 62 (2008), pp. 789–798.

[13] E.S. Gurdjian, H.R. Lissner, F.R. Latimerr, B.F. Haddad, and J.E. Webster, *Quantitative determination of acceleration and intercranial pressure in experimental head injury*, Neurology 3 (1983), pp. 417–423.

[14] E.S. Gurdjian, V.L. Roberts, and L.M. Thomas, *Tolerance curves of acceleration and intracranial pressure protective index in experimental head injury*, J. Trauma 6 (1966), pp. 600–604.

[15] Insurance Institute for Highway Safety, *Moderate Overlap Frontal Crashworthiness Evaluation: Guidelines for Rating Injury Measures*, Insurance Institute for Highway Safety, Arlington, VA, 2014.

[16] T. Kapoor, W. Altenhof, A. Howard, A. Snowdon, J. Rasico, F. Zhu, and K. Mizuno, *Countermeasures to mitigate head and neck injuries to toddlers in frontal and lateral vehicle crash conditions*, Int. J. Crashworthiness 15 (2010), pp. 17–37.

[17] H. Kimpara and M. Iwamoto, *Mild traumatic brain injury predictors based on angular accelerations during impacts*, Ann. Biomed. Eng. 40 (2012), pp. 114–126.

[18] S. Kleiven, *Evaluation of head injury criteria using a finite element model validated against experiments on localized brain motion, intracerebral acceleration, and intracranial pressure*, Int. J. Crashworthiness 11 (2006), pp. 65–79.

[19] S. Kleiven, *A parametric study of energy absorbing foams for head injury prevention*, Proceedings of the 20th Interational Technical Conference on Enhanced Safety of Vehicles, 2007, pp. 18–21.

[20] B.R. Kretz, K. Hausberger, B. Götzinger, and S.F. Ag, *Energy-absorbing behavior of aluminum foams : Head impact tests on the a-pillar of a car*, Adv Eng Mater. 4 (2002), pp. 781–785.

[21] L.M. Lewis, R.S. Naunheim, J. Standeven, and K.S. Naunheim, *Quantitation of impact attenuation of different playground surfaces under various environmental conditions using a tri-axial accelerometer*, J. Trauma 35 (1993), pp. 932–935.

[22] S.S. Margulies and L.E. Thibault, *A proposed tolerance criterion for diffuse axonal injury in man*, J. Biomech. 25 (1992), pp. 917–923.

[23] D. Marjoux, D. Baumgartner, C. Deck, and R. Willinger, *Head injury prediction capability of the HIC, HIP, SIMon and ULP criteria*, Accident Anal. Prevention 40 (2008), pp. 1135–1148.

[24] W.C. Moss and M.J. King, *Impact response of US Army and National Football League helmet pad systems*, Lawrence Livermore National Labs Special Report LLNL-SR-464951, 2011.

[25] N.J. Mills, C. Fitzgerald, A. Gilchrist, and R. Verdejo, *Polymer foams for personal protection: Cushions, shoes and helmets*, Compos. Sci. Technol. 63 (2003), pp. 2389–2400.

[26] R.S. Naunheim, J. Standeven, C. Richter, and L.M. Lewis, *Comparison of impact data in hockey, football, and soccer*, J. Trauma 48 (2000), pp. 938–941.

[27] J.A. Newman, N. Shewchenko, and E. Welbourne, *A proposed new biomechanical head injury assessment function – the maximum power index*, Stapp Car Crash J. 44 (2000), pp. 1–33.

[28] E.J. Pellman, D.C. Viano, A.M. Tucker, I.R. Casson, and J. F. Waeckerle, *Concussion in professional football: Reconstruction of game impacts and injuries*, Neurosurgery 53 (2003), pp. 799–814.

[29] J.S. Raul, D. Baumgartner, R. Willinger, and B. Ludes, *Finite element modelling of human head injuries caused by a fall*, Int. J. Legal Med. 120 (2006), pp. 212–8.

[30] A.A. Sabet, E. Christoforou, B. Zatlin, G.M. Genin, and P. V. Bayly, *Deformation of the human brain induced by mild angular head acceleration*, J. Biomech. 41 (2008), pp. 307–315.

[31] B. Shields and G.A. Smith, *The potential for brain injury on selected surfaces used by cheerleaders*, J. Athletic Training 44 (2009), pp. 595–602.

[32] E.G. Takhounts, M.J. Craig, K. Moorhouse, and J. Mcfadden, *Development of Brain Injury Criteria (BrIC)*, Stapp Car Crash J. 57 (2010), pp. 243–266.

[33] U.S. Department of Transportation, *Federal Motor Vehicle Safety Standards*, Standard 208, Washington, DC, 2014.

[34] J. Versace, *A review of the severity index*, Proceedings of the 15th Stapp Car Crash Conference (SAE Paper 710881), 1971.

[35] M. Vander Vorst, J. Stuhmiller, K. Ho, N. Yoganandan, and F. Pintar, *Statistically and biomechanically based criterion for impact-induced skull fracture*, Annu. Proc. Assoc. Advancement Automotive Med. 47 (2003), pp. 363–381.

[36] R. Willinger and D. Baumgartner, *Human head tolerance limits to specific injury mechanisms*, Int. J. Crashworthiness 8 (2003), pp. 605–617.
[37] S. Yin, A.J. Jacobsen, L. Wu, and S.R. Nutt, *Inertial stabilization of flexible polymer micro-lattice materials*, J. Mater. Sci. 48 (2013), pp. 6558–6566.
[38] J. Zhang, N. Yoganandan, and F.a. Pintar, *Dynamic biomechanics of the human head in lateral impacts*, Ann. Adv. Automotive Med. 53 (2009), pp. 249–56.
[39] L. Zhang, M. Gurao, K.H. Yang, and A.I. King, *Material characterization and computer model simulation of low density polyurethane foam used in a rodent traumatic brain injury model*, J. Neurosci. Methods 198 (2011), pp. 93–98.
[40] W. Zhao, S. Ruan, and S. Ji, *Brain pressure responses in translational head impact: A dimensional analysis and a further computational study*, Biomech. Model. Mechanobiol. (2014). doi:10.1007/s10237-014-0634-0
[41] ASTM Standard F1292, *Standard Specification for Impact Attenuation of Surfacing Materials within the Use Zone of Playground Equipment*, ASTM Int., West Conshohocken, PA, 2009.